

Open-boundary Hamiltonian adaptive resolution. From grand canonical to non-equilibrium molecular dynamics simulations

Cite as: J. Chem. Phys. **152**, 194104 (2020); <https://doi.org/10.1063/1.5143268>

Submitted: 20 December 2019 . Accepted: 27 April 2020 . Published Online: 19 May 2020

Maziar Heidari , Kurt Kremer , Ramin Golestanian , Raffaello Potestio , and Robinson Cortes-Huerto 



View Online



Export Citation



CrossMark

ARTICLES YOU MAY BE INTERESTED IN

[CP2K: An electronic structure and molecular dynamics software package - Quickstep: Efficient and accurate electronic structure calculations](#)

The Journal of Chemical Physics **152**, 194103 (2020); <https://doi.org/10.1063/5.0007045>

[Single trajectory transport coefficients and the energy landscape by molecular dynamics simulations](#)

The Journal of Chemical Physics **152**, 194504 (2020); <https://doi.org/10.1063/5.0005600>

[Ensemble learning of coarse-grained molecular dynamics force fields with a kernel approach](#)

The Journal of Chemical Physics **152**, 194106 (2020); <https://doi.org/10.1063/5.0007276>

Lock-in Amplifiers
up to 600 MHz



Open-boundary Hamiltonian adaptive resolution. From grand canonical to non-equilibrium molecular dynamics simulations

Cite as: J. Chem. Phys. 152, 194104 (2020); doi: 10.1063/1.5143268

Submitted: 20 December 2019 • Accepted: 27 April 2020 •

Published Online: 19 May 2020



View Online



Export Citation



CrossMark

Maziar Heidari,¹  Kurt Kremer,¹  Ramin Golestanian,^{2,3}  Raffaello Potestio,^{4,5,a)} 
and Robinson Cortes-Huerto^{1,b)} 

AFFILIATIONS

¹Max Planck Institute for Polymer Research, Ackermannweg 10, 55128 Mainz, Germany

²Max Planck Institute for Dynamics and Self-Organization (MPIDS), 37077 Göttingen, Germany

³Rudolf Peierls Centre for Theoretical Physics, University of Oxford, Oxford OX1 3PU, United Kingdom

⁴Physics Department, University of Trento, Via Sommarive, 14, I-38123 Trento, Italy

⁵INFN-TIFPA, Trento Institute for Fundamental Physics and Applications, I-38123 Trento, Italy

^{a)}E-mail: raffaello.potestio@unitn.it

^{b)}Author to whom correspondence should be addressed: corteshu@mpip-mainz.mpg.de

ABSTRACT

We propose an open-boundary molecular dynamics method in which an atomistic system is in contact with an infinite particle reservoir at constant temperature, volume, and chemical potential. In practice, following the Hamiltonian adaptive resolution strategy, the system is partitioned into a domain of interest and a reservoir of non-interacting, ideal gas particles. An external potential, applied only in the interfacial region, balances the excess chemical potential of the system. To ensure that the size of the reservoir is infinite, we introduce a particle insertion/deletion algorithm to control the density in the ideal gas region. We show that it is possible to study non-equilibrium phenomena with this open-boundary molecular dynamics method. To this aim, we consider a prototypical confined liquid under the influence of an external constant density gradient. The resulting pressure-driven flow across the atomistic system exhibits a velocity profile consistent with the corresponding solution of the Navier–Stokes equation. This method conserves, on average, linear momentum and closely resembles experimental conditions. Moreover, it can be used to study various direct and indirect out-of-equilibrium conditions in complex molecular systems.

© 2020 Author(s). All article content, except where otherwise noted, is licensed under a Creative Commons Attribution (CC BY) license (<http://creativecommons.org/licenses/by/4.0/>). <https://doi.org/10.1063/1.5143268>

I. INTRODUCTION

Computational and experimental communities routinely cooperate by comparing the results obtained from their respective methods. However, such comparisons are intrinsically limited in scope because real systems approach the thermodynamic limit, whereas model systems usually have a finite number of particles. Indeed, standard computer simulations frequently consider closed systems whose fixed number of particles introduces finite-size effects due to the *de facto* simultaneous use of different statistical ensembles.^{1–3}

With the computational power nowadays available, it is tempting to ask whether it is possible to increase the size of the system and safely ignore ensemble finite-size effects, i.e., reach the thermodynamic limit. In particular, for a system of total number of particles N_0 at temperature T in a volume V_0 , it is possible to consider a subdomain of volume V with an average number of particles $\langle N \rangle$. The system can be considered in the grand canonical ensemble if V is of the order of 1% of the total volume V_0 .⁴ This size constraint implies using huge simulation boxes which, in most cases, demand tremendous computational effort.

A simplification of the physical representation of the particles in the reservoir alleviates this computational load. This idea is the essence of the adaptive resolution method: an atomistic (AT) subdomain of volume V , defined within the simulation box, is in contact with a reservoir of coarse-grained (CG) particles.^{5–9} A smooth interpolation between atomistic and coarse-grained forces, acting on molecules present at the interface between the two regions, ensures a consistent description of the whole system. Indeed, the adaptive resolution framework is a robust method to perform simulations in the grand canonical ensemble.^{10–15} To build upon these results, we discuss two components that one should consider to make use of the adaptive resolution method to perform well-controlled open-boundary molecular dynamics simulations.

First, a simulation in the μVT ensemble requires beforehand knowledge of the chemical potential μ of the bath. This condition is analogous to the situation in the NVT ensemble in which one first requires to fix the number of particles N . In the original adaptive resolution framework, it is possible to obtain the difference in chemical potential between atomistic and coarse-grained representations of the system.¹⁶ If one knows the chemical potential of the coarse-grained model, then it is straightforward to obtain and control μ for the atomistic one. It is thus convenient to use the simplest possible coarse-grained representation such that the calculation of the chemical potential does not involve an additional external computation.

Second, a system is in the grand canonical ensemble if it is in thermal and chemical equilibrium with an infinite particle reservoir. Computer memory limitations prevent the possibility to consider an infinite number of particles. Instead, a particle insertion/deletion algorithm coupled to the simulation setup effectively ensures this requirement by allowing the interchange of particles with an infinite ideal gas (IG) reservoir. In the context of the adaptive resolution method, a semi-grand canonical method was proposed to illustrate this point.¹² The idea to interpret the adaptive resolution methodology in terms of a simulation with a particle reservoir was first formulated in Ref. 11. This identification of the coarse-grained system is completely general as illustrated in the case of atomistic/mesoscopic continuum adaptive resolution models^{17,18} in which open boundary conditions can be readily enforced.^{19–21} Nevertheless, the sampling resulting from particle insertion/deletion events, even if only applied in the coarse-grained region, becomes less representative as the density, concentration, and complexity of the system increase.

To consider these points, here we present a method that combines a particle insertion/deletion algorithm with the Hamiltonian adaptive resolution framework (H-AdResS).^{22,23} Following the method suggested in Ref. 24, we replace the coarse-grained model by a reservoir of non-interacting thermalized particles (ideal gas). In this case, the applied external potential used to ensure a uniform density through the simulation box balances the excess chemical potential of the atomistic model. Therefore, the atomistic system is at constant chemical potential with a reservoir of ideal gas particles. We introduce the particle insertion/deletion algorithm, operating on the ideal gas reservoir, to overcome the limitations existing on available methods due to high density/concentration and system complexity conditions. The method is thus capable of performing constant μ molecular dynamics simulations without the necessity to include external forces and to compensate for depletion of particles in the reservoir.^{25–27}

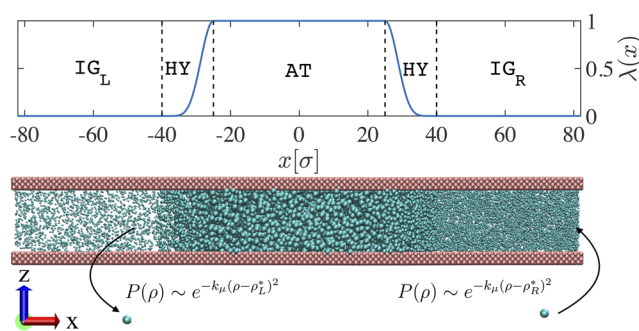


FIG. 1. Hamiltonian adaptive resolution setup used to simulate a liquid confined between parallel plates. Upper panel: the simulation box is partitioned into atomistic (AT), hybrid (HY), and two unconnected left and right reservoirs of ideal gas ($IG_{L/R}$) particles. The identity of the molecules is defined by the switching function $\lambda(x)$ that takes values between 0 and 1. Lower panel: simulation snapshot explicitly showing the confined liquid in the various subdomains. For this particular example, the number density is lower in the IG_L than in the IG_R region.

There is a permanent and ongoing interest in simulating non-equilibrium phenomena in inhomogeneous fluids.^{28–42} With the open-boundary molecular dynamics method proposed here, it is possible to investigate such phenomena. In particular, we consider a confined liquid such that its ideal gas reservoir is under the influence of a constant density gradient. Initially, a uniform density profile is enforced parallel to the surfaces (see Fig. 1). Upon equilibration, a density gradient imposed in the reservoir induces a pressure-driven flow in the system with a velocity profile consistent with the corresponding solution of the Navier–Stokes equation. The method closely resembles experimental conditions and conserves, on average, linear momentum. Furthermore, the intrinsic arbitrariness of the ideal gas reservoir opens the possibility to study various direct and indirect non-equilibrium conditions.

The paper is organized as follows: In Sec. II, we validate the use of H-AdResS to study confined liquids and introduce the particle insertion/deletion algorithm. We present the results for pressure-driven flow in Sec. III, and finally, discuss, conclude, and outline research directions in Sec. IV.

II. MODEL

In adaptive resolution simulations, it is possible to couple a target system with an ideal gas reservoir of particles at constant chemical potential.^{24,43} Particularly, it is possible to set the chemical potential of the target system by controlling the number density in the ideal gas reservoir. In this work, we implement a particle insertion algorithm that operates on the ideal gas region and permits fluctuations in the number density around a target value. Consequently, the standard H-AdResS setup now allows one to perform open-system molecular dynamics simulations in equilibrium and, more importantly, nonequilibrium conditions. As an illustration, we study the prototypical example of liquid flow across a narrow channel. All simulations are performed with the LAMMPS simulation package,^{44,45} where the method is implemented.

Before introducing the particle insertion algorithm, we validate H-AdResS to study a confined liquid between parallel walls.

A. H-AdResS for a confined liquid

Let us consider a single component liquid confined between parallel walls with normal perpendicular to the x -axis and separated by a distance D . In the adaptive resolution method (AdResS),^{5–7} atomistic (AT) and coarse grained (CG) representations of the system are concurrently present in the simulation box and coexist in thermodynamic equilibrium.^{5–7} In particular, by using a position-dependent switching field $\lambda(x)$ (see Fig. 1), it is possible to write a Hamiltonian (H-AdResS)^{22,23} for the whole system. Since AT and CG representations of the system follow different equations of state, an additional term is included in the Hamiltonian to guarantee a constant density (implying constant chemical potential) across the simulation box. Finally, the choice of the coarse grained representation is rather arbitrary and can even be reduced to a reservoir of noninteracting—ideal gas (IG)—particles.^{24,43} In this context, we write the Hamiltonian for a system composed of $N = N_s + N_w$ solvent (s) and wall (w) molecules as⁴⁶

$$H_{[\lambda]}(r, p) = K + V^w(r) + V_{[\lambda]}(r), \quad (1)$$

with (r, p) being the positions and momenta and $K = \sum_{i=1}^N \mathbf{p}_i^2 / 2m_i$ being the total kinetic energy of the system. The term

$$V^w(r) = \frac{\kappa}{2} \sum_{\substack{j \neq j' \\ j, j' \in w}} (r_{j, j'} - r_0)^2$$

is a harmonic, nearest-neighbour $V^w(r > r_{\text{cut}}) = 0$ potential used to restrain the position of the wall molecules. κ is the spring constant, r_0 is the equilibrium length, and $r_{j, j'}$ is the distance between a given pair of wall particles. The wall particles are located on a fcc lattice of density $0.9 \sigma^{-3}$ with parameters $\kappa = 1000 \epsilon \sigma^{-2}$ and $r_0 = 1.1626 \sigma$. $V^w(r)$ is only applied during the initial equilibration. For production runs, the surface particles are frozen in their final equilibrium positions. We impose this constraint to solve a technical problem, namely, due to the pressure imbalance present between the AT and IG regions, the wall might deform and its elastic response could affect the behavior of the solvent. Moreover, this constraint enforces no-slip conditions in the system. Indeed, thermal fluctuations of wall particles enhance the decoupling of wall–fluid interactions, thus increasing the slip length.³⁰

The last term in the Hamiltonian (1) is written as

$$V_{[\lambda]}(r) = \sum_{\substack{i=1 \\ i \in s}}^{N_s} \lambda_i \left[\frac{1}{2} \sum_{\substack{i'=1 \\ i' \neq i}}^{N_s} U^{s, s}(r_{i, i'}) + \sum_{\substack{j=1 \\ j \in w}}^{N_w} U^{s, w}(r_{i, j}) \right] + (1 - \lambda_i) \sum_{\substack{j=1 \\ j \in w}}^{N_w} U^{\text{ig}, w}(r_{i, j}) - \Delta H^s(\lambda_i). \quad (2)$$

The solvent molecules i interact via an intermolecular potential modulated by a switching field $\lambda_i \equiv \lambda(x_i)$ (see Fig. 1). The switching field takes values 0 in the IG region where solvent particles only interact repulsively with wall particles and 1 in the AT region where solvent particles fully interact with both solvent and wall particles. A smooth interpolation between 0 and 1 is defined in the hybrid

(HY) region. The free energy compensation (FEC) term, ΔH^s , is introduced in the Hamiltonian to compensate non-physical, drift forces due to gradients of the switching field. Moreover, it ensures momentum conservation *on average* and guarantees a uniform density throughout the simulation box. Note that the FEC is only applied to confined liquid particles instantaneously present in the hybrid region. The starting point of the simulations corresponds to a fully atomistic case. Once these simulations are equilibrated, the adaptive resolution setup is turned on and ΔH^s is computed *on-the-fly* following the procedure described in Ref. 45 included in the equilibration of the H-AdResS run. Finally, for homogeneous systems, $\Delta H^s(\lambda = 1)$ corresponds to the system's excess chemical potential μ_{exc} . This procedure has been identified with a thermodynamic integration in space, i.e., spatially resolved thermodynamic integration (SPARTIAN).²⁴

We model all the solvent–wall interactions with the truncated and shifted Lennard-Jones potential,

$$U^{\alpha, \beta}(r) = 4\epsilon_{\alpha, \beta} \left[\left(\frac{\sigma_{\alpha, \beta}}{r} \right)^{12} - \left(\frac{\sigma_{\alpha, \beta}}{r} \right)^6 \right], \quad (3)$$

where the units of length, energy, and mass are defined by the parameters σ , ϵ , and m , respectively. In the following, we report the results in Lennard-Jones (LJ) units with time $\tau = \sigma(m/\epsilon)^{1/2}$, temperature ϵ/k_B , and pressure ϵ/σ^3 . For a given cutoff radius r_{cut} , the value $U^{\alpha, \beta}(r_{\text{cut}})$ is evaluated and subtracted from Eq. (3). The parameters used to describe all interactions between species (α, β) for different regions within the simulation box are presented in Table I with fixed solvent–solvent (s,s) and ideal gas–wall (ig,w) values. For solvent–wall (s,w) interactions in the AT region, we consider the purely repulsive Lennard-Jones potential (WCA) as well as the truncated and shifted Lennard-Jones potential with $r_{\text{cut}} = 2.5 \sigma$ with varying interaction strength modulated by the parameter η with $\eta = 0.5, 1.0, 1.5, 2.0$, and 2.5 .

In this example, the number of solvent and wall particles is fixed with $N_s = 97\,020$ and $N_w = 48\,000$, respectively. The size of the box is set by $L_x = 164.41 \sigma$ and $L_y = 49.32 \sigma$, while L_z is fixed by the system's pressure with variations in the range of $L_z = 24.75 \sigma, \dots, 25.61 \sigma$. For the case of homogeneous liquid, i.e., no confining walls, $L_z = 18.74 \sigma$. The initial fully atomistic equilibration is carried out in the NPT ensemble using the Nose–Hoover thermostat and barostat for 5000τ with time step size of $\delta t = 10^{-3} \tau$. The temperature is fixed at $k_B T = 2.0 \epsilon$ with damping coefficient 10τ and the pressure is fixed anisotropically at $P = 2.65 \epsilon \sigma^{-3}$ with damping coefficient 100τ by applying a force normal to the walls. The final equilibrium density, which is defined as the ratio of number of liquid particles to the total

TABLE I. Lennard-Jones parameters used to describe solvent–solvent and solvent–wall interactions. Additionally, to the purely repulsive case (not included in this table), the latter interactions are modulated in the AT region by the parameter η , whereas in the IG region is defined as purely repulsive.

(α, β)	$\epsilon_{\alpha, \beta}$	$\sigma_{\alpha, \beta}$	$r_{\alpha, \beta}^{\text{cut}}$
(s,s)	ϵ	σ	2.5σ
(s,w)	$\eta \epsilon$	σ	2.5σ
(ig,w)	ϵ	σ	$2^{1/6} \sigma$

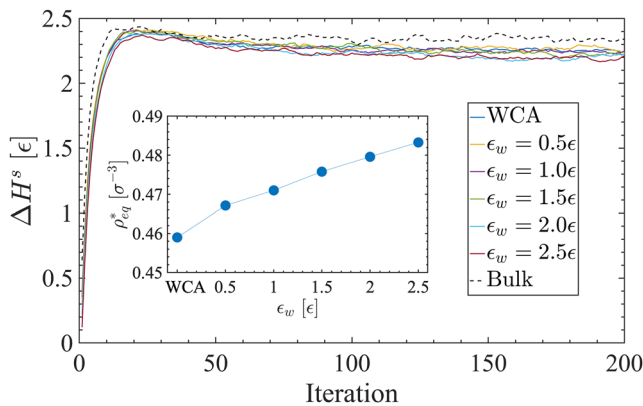


FIG. 2. The convergence of compensating energies of the LJ fluid for different fluid–wall interactions as obtained by the method outlined in Ref. 24. In all cases, the initial configuration is equilibrated at the same pressure $P = 2.65 \epsilon \sigma^{-3}$ and temperature $k_B T = 2.0 \epsilon$. Inset shows the final equilibrium densities obtained from fully atomistic simulations of the systems.

volume of the simulation box ($\rho_{eq}^* = N_s/V$), is reported in the inset of Fig. 2 for different fluid–wall interactions. This definition of density is useful, however, arbitrary. The volume accessible to the fluid cannot be uniquely determined because the definition of the contact surface between the fluid and the walls is somewhat unclear.³¹

To validate the reliability of H-AdResS to study confined liquids, we verify that the FEC terms, ΔH^s , converge. The size of AT and HY regions is 50σ and 15σ and the H-AdResS parameters are listed in Table II. As mentioned before, the application of the FEC on the system leads to a constant density profile across the simulation box. In this case, the system reaches an equilibrium state in which atomistic and ideal gas particles have equal chemical potential. The evolution of the FEC as a function of time is plotted in Fig. 2. After 200 iterations, which corresponds to 2000τ simulation time (see Table II for more detail), the algorithm converges to $\mu = 2.33 \pm 0.008 \epsilon$ for the bulk liquid (no confinement), in a good agreement with the previously reported value for LJ fluid ($\mu = 2.33 \pm 0.01 \epsilon^{24}$).

TABLE II. H-AdResS parameters for LJ and WCA fluids. The first two rows correspond to the parameters being used in time sampling of drift and thermodynamic forces (t_{smp}^{dr} and t_{smp}^{th}) as well as their averaging process (t_{ave}^{dr} and t_{ave}^{th}). The values are presented in a number of time steps. The second two rows enlist the size of the bins in discretization of the HY region to obtain the drift force ($\Delta\lambda$) and thermodynamic force (ΔX). The parameters being used in the convolution of the density profile with the Gaussian function are the thermodynamic scaling factor (c), reference number density (ρ^*), the standard deviation of the Gaussian function (σ_ρ), and the domain of convolution integration (l). Details about the precise meaning of these parameters can be found in Ref. 24.

Δt_{smp}^{dr}	Δt_{smp}^{th}	Δt_{ave}^{dr}	Δt_{ave}^{th}	δt	Iterations
100	100	5×10^4	5×10^4	$10^{-3} \tau$	200
$\Delta\lambda$	$\Delta X[\sigma]$	$c[\epsilon]$	$\rho^*[\sigma^{-3}]$	$\sigma_\rho[\sigma]$	$l[\sigma]$
0.005	0.5	1.0	0.5	2.0	4.0

To investigate the structure of the liquid inside the AT region, we calculate the equilibrium particle distribution function normal to the wall, $g(z)$, and compare it with the results obtained from the fully atomistic simulation. The distribution function is obtained by binning the atomistic region along the z -axis and time averaging over all bins with equal z -coordinate. As shown in Fig. 3, the surface-induced layering structure is well reproduced by the H-AdResS simulation. Moreover, the comparison of the bulk particle distribution [$g(z)$; for $|z| < 5\sigma$] shows that the density of the atomistic region in the adaptive setup has converged to the atomistic reference density. These results confirm the suitability of our method to study confined liquids under the conditions here specified.

It has been demonstrated that for a liquid in equilibrium at a given temperature T and composed of N molecules inside a container of volume V , the chemical potential equals the chemical potential of the uniform system.⁴⁷ However, as mentioned before, the definition of the volume available to the fluid is ambiguous.³¹ For such a reason, we avoid identifying the free energy compensation ΔH^s with the excess chemical potential of the uniform system. Hence, in Sec. II B, to precisely enforce a constant chemical potential in an open system, we introduce and validate the particle insertion algorithm for a bulk liquid system.

B. Particle insertion algorithm

The proposed grand canonical molecular dynamics method consist of two parts: first, the AT/IG constant chemical potential coupling that has been already discussed in Sec. II A, as well as in Ref. 24. Second, we allow particle exchange between the IG region and an ideal gas reservoir used to control the chemical potential of the system. The details of the particle insertion algorithm applied on the IG region are the subject of this section.

We start by assuming that the IG region is in the grand canonical ensemble. The probability that the IG region, at temperature T , volume V_0 , and chemical potential μ , has exactly N particles follows the Poisson distribution⁴⁸

$$P(N) = \frac{(N^*)^N e^{-N^*}}{N!}, \quad (4)$$

with N^* being the mean number of particles in the volume V_0 . In the ideal gas case, N^* can be written in terms of the chemical potential of the system,

$$N^* = \frac{V_0 e^{\beta\mu}}{\lambda^3}, \quad (5)$$

with $\beta = 1/k_B T$ and λ being the mean thermal wavelength. In the limit $N, N^* \gg 1$ with $|(N - N^*)/N^*| \ll 1$, we obtain

$$P(N) = \frac{e^{-(N-N^*)^2/2N^*}}{\sqrt{2\pi N^*}}. \quad (6)$$

This is a normal distribution with mean value N^* and standard deviation $\sqrt{N^*}$. In physical terms, this corresponds to the well-known result for the isothermal compressibility κ of the ideal gas, i.e., $\kappa = 1/\rho k_B T$ with $\rho^* = N^*/V_0$. We are interested in fluctuations around a target density ρ^* ; therefore, we rewrite $P(N)$ in terms of $\rho = N/V_0$ as

$$P(\rho) \sim e^{-k_\mu(\rho - \rho^*)^2/2}, \quad (7)$$

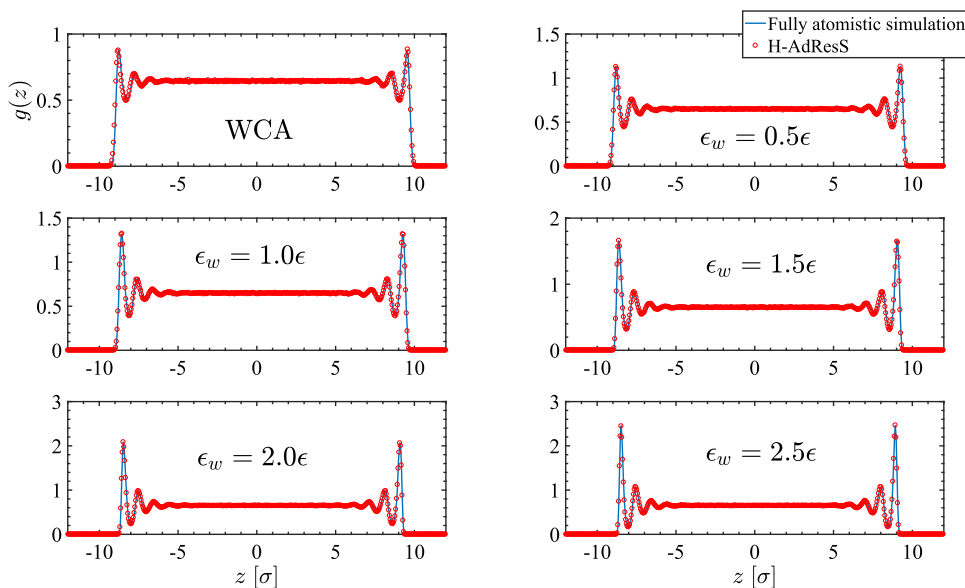


FIG. 3. Particle density profiles normal to the wall surface obtained for the LJ fluid with different wall interactions. The results are presented for the fully atomistic simulation and H-AdResS.

where, in principle, $k_\mu = V_0/\rho^*$, but in the following, we treat it as a free parameter related to the width of the distribution of possible values for the target density ρ^* . With this probability distribution, we introduce the Metropolis algorithm used for particle insertion. The probability to accept a move that the present density ρ increases by v is given by

$$\text{acc}(\rho \rightarrow \rho + v) = \min[1, \exp(-k_\mu v(\rho + 2(\rho - \rho^*)))], \quad (8)$$

and correspondingly,

$$\text{acc}(\rho \rightarrow \rho - v) = \min[1, \exp(-k_\mu v(\rho - 2(\rho - \rho^*)))]. \quad (9)$$

Concerning the fluctuations around the target density, we select values of v according to the normal distribution

$$P(v) = \sqrt{\frac{k_\mu}{2\pi}} e^{-\frac{k_\mu v^2}{2}}. \quad (10)$$

Finally, the particle insertion Monte Carlo moves are performed every ΔT_{exch} time steps during which the number of particles is averaged.

In conventional grand canonical simulations, the target system can interchange particles with an infinite ideal gas reservoir at constant chemical potential.⁴⁹ Alternatively, the atomistic/coarse-grained coupling present in adaptive resolution simulations provides a suitable playground to sample the grand canonical ensemble.^{10–15} In our particular case, the size of the reservoir can be substantially increased since particles in the IG region are non-interacting.^{24,43} Alternatively, by introducing density fluctuations in the IG region, we also ensure interchange of particles with an infinite reservoir of ideal gas particles at constant chemical potential.

To verify grand canonical conditions, we run an equilibrium simulation for a bulk LJ liquid, i.e., with the confining walls removed, at a given pressure $P = 2.65 \epsilon \sigma^{-3}$ and temperature $k_B T = 2 \epsilon$. These

conditions define the target density $\rho_{\text{eq}}^* = 0.647 \sigma^{-3}$ and the corresponding chemical potential. Upon obtaining the equilibrated all-atom configuration, “ghost” particles are placed in each reservoir, and then, H-AdResS is performed using the Hamiltonian of Eq. (1) and the obtained FEC terms corresponding to the target density. The velocity and force of the ghost particles are set to zero, so they do not move during the H-AdResS parameterization runs. The *on the fly* calculation of compensation of the drift and thermodynamic forces are updated every 5×10^4 time steps, during 10×10^6 time steps (200 iterations). The resolution interval is divided into 200 bins of size $\Delta\lambda = 0.005$ and the length of the simulation box is uniformly discretized into slabs of size $\Delta x = 0.5 \sigma$. We employed values of $c = 1 \epsilon$, $\sigma_\rho = 2 \sigma$, and $l = 4 \sigma$ for smoothing and scaling the thermodynamic force.

To verify that the particle insertion protocol drives the system to a target density, ρ^* , we start with two versions of the system at the same temperature, but one at lower, $\rho < \rho^*$, and the other at higher, $\rho > \rho^*$, density.^{50,51} In both cases, we apply the FEC obtained from the target system to set the target chemical potential and run the open boundary simulation using ρ^* as an input for the particle insertion protocol. In Fig. 4, the evolution of density as a function of simulation time is presented in both cases, $\rho_{\text{L,R}}^{\text{IG}} < \rho^*$ (a) and $\rho_{\text{L,R}}^{\text{IG}} > \rho^*$ (b).

It is apparent from Fig. 4 that the density in the three regions, left, right, and AT, converges to the reference density in all cases, independently of the choice of insertion frequency k_μ . In general, this result verifies that the open simulation setup described corresponds to a constant chemical potential molecular dynamics simulation. The behavior at short times indicates that the FEC works to restore the density in the atomistic region (dashed lines) by depleting (a)/increasing (b) the number of particles in the reservoir. The effect of the particle insertion algorithm is thus to bring the density of the reservoir (solid and dotted lines) to the target value and equate the chemical potential across different simulation regions. Finally,

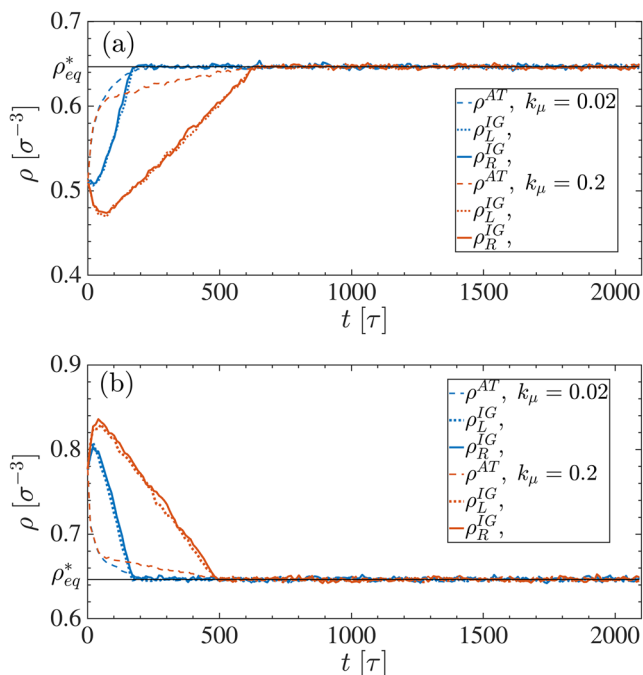


FIG. 4. Evolution of the density in the left (ρ_L^{IG}) and right (ρ_R^{IG}) ideal gas regions and atomistic (ρ^{AT}) regions when the system has initially lower (a) or higher (b) density than the equilibrium reference density (ρ_{eq}^*).

the behavior of the system as a function of k_μ is consistent with the interpretation given in terms of the width of the distribution of ρ^* .

In the final section, we return to the confined liquid problem and use the particle insertion algorithm in a nonequilibrium molecular dynamics setup to induce a density gradient throughout the system.

III. INDUCED DENSITY GRADIENT AND PLANE POISEUILLE FLOW

In this section, we start with the equilibrated configurations for the confined liquid considered in Sec. II A. We remove the periodic boundary conditions along the x direction to decouple left and right reservoirs and introduce repulsive walls to confine the ideal gas particles. We use the Langevin thermostat to control the temperature in all regions at $k_B T = 2 \epsilon$ with damping coefficient 10τ . The time step is $\delta t = 10^{-3} \tau$, and for each case, the total simulation run is 14×10^6 time steps. To induce the density gradient between the atomistic region and ideal gas reservoirs, the particle exchange algorithm is applied independently in each reservoir. The reference number densities of particles in the left reservoir is set as the equilibrium number density $\rho_L^* = \rho_{eq}^*$. The reference number density in the right reservoir is increased with respect to the equilibrium number density. We use $k_\mu = 0.1 \epsilon$ and $\Delta T_{exch} = 100 \delta t$ for all simulation sets. The reservoir (frozen) particles are also exchanged between the two reservoirs every 100 time steps to balance the number of particles in the reservoirs.

The combination of inducing a density gradient and enforcing a reference density generates an excess of frozen particles in the

left reservoir. To keep the simulation running, we periodically relocate these frozen particles from left to right reservoirs. This technical aspect does not affect our results since frozen particles have zero momentum.

As both reservoirs are confined by repulsive walls, the number density of each reservoir is calculated over a smaller control volume than V_{IG} , which does not contain the depletion layer close to the right and left repulsive walls. Additionally, the width of the depletion layers changes when the solvent changes from LJ fluid (fully atomistic simulation) to ideal gas particles (H-AdResS), which changes the total available volume. This difference in volume can be compensated by increasing the hard core size of the repulsive LJ potential between the walls and ideal gas particle such that the number density far from the depletion zone equals the one in fully atomistic simulations. In our study, however, such difference is negligible.

Concerning statistics, all values are reported using the block averaging method. For each case, we divide the total simulation run into seven uniform blocks of 2×10^6 time steps each. To remove the effect of the transient behavior, we do not consider the results of the first block (see the inset of Fig. 5). The average values of each block are calculated, and then, we report the average and standard deviation values of all blocks.

Figure 5 shows the number density profile of particles when the system reaches the steady state (as shown in the inset). It is apparent that the induced density gradient in the atomistic region and the ripples observed there are generated by the interaction with the surface. As expected, the difference in densities between the right and left reservoirs is equal to the actual nominal difference. The density profile at the IG_L/HY interface exhibits bumps that become more distinct upon increasing the density gradient. These can be attributed to a mismatch in mobility due to particles changing identity from atomistic to non-interacting. Thus, particles accumulate before entering the left reservoir, and once there, the particle insertion algorithm flattens the profile to reach the reference density.

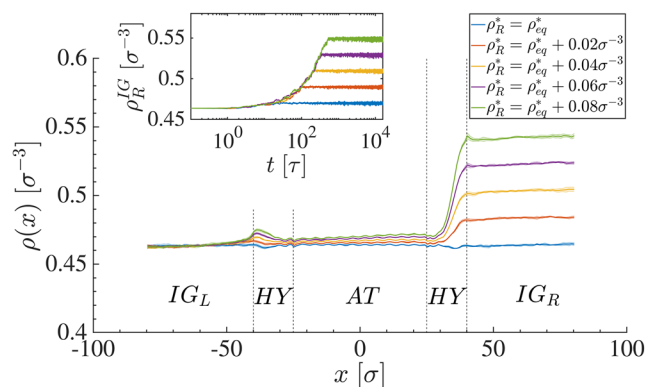


FIG. 5. Number density profiles shown for different reference values ρ_R^* . In all cases, the reference number density in the left reservoir is set to the equilibrium reference number density ρ_{eq}^* . Inset shows the time evolution of the number density in the right reservoir.

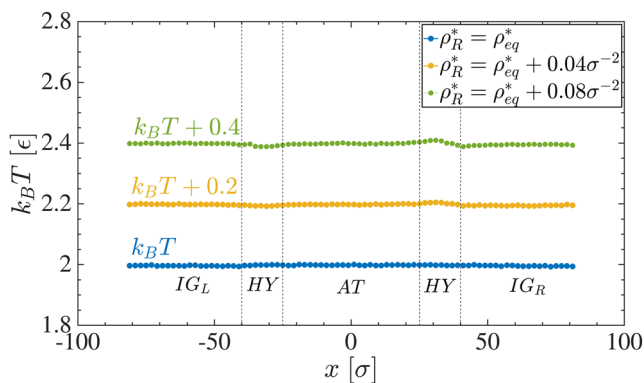


FIG. 6. Temperature profiles of the system when the fluid–wall interaction strength is $\epsilon_w = 2 \epsilon$. For clarity, the profiles have been shifted by a constant quantity.

To effectively isolate the effect of the induced density gradient in the atomistic region, it is necessary to guarantee that the temperature is constant throughout the simulation box. This is presented in Fig. 6, clearly indicating a uniform temperature of the entire system. As a matter of fact, the maximum deviation of temperature from the mean value occurs in the case of induction of the largest density gradient and it is 0.015ϵ (less than 1% of the mean temperature). This is found to be in the middle of the hybrid region where the resolution of the ideal gas changes effectively into LJ fluid.

At this point, we are in the position to compare our simulation results with hydrodynamics, namely, the Poiseuille flow equation.⁵² A simple dimensional analysis justifies such a comparison. To this end, we employ the Knudsen number, defined as $\text{Kn} = \lambda/D_h$ with $\lambda = 1/\sqrt{2}\rho\pi\sigma^2$ being the mean free path of the fluid particles and $D_h = 20 \sigma$ being the height of the channel. Knudsen numbers for the system under consideration vary between $\text{Kn} = 0.014, \dots, 0.016$, indicating that a parallel can be drawn between continuum fluid dynamics and our simulation results.⁵³

A plane Poiseuille flow is created in a fluid with density ρ and dynamic viscosity η confined between infinitely long parallel plates, separated by a distance D_h , when a constant pressure gradient is applied along the axis of the channel x . The resulting flow is unidirectional. At low Reynolds number, the Navier–Stokes equation can be written as

$$\frac{d^2 u_x(z)}{dz^2} = \frac{1}{\eta} \frac{\Delta p}{\Delta x}, \quad (11)$$

where the axial velocity $u_x(z)$ is only a function of the z -coordinate and the applied pressure gradient $\Delta p/\Delta x$ is constant. Using the

boundary conditions $u_x(z = \pm D_h/2) = 0$ (no-slip condition), we obtain

$$u_x(z) = \frac{1}{\eta} \frac{\Delta p}{\Delta x} \left[z^2 - \frac{D_h^2}{4} \right]. \quad (12)$$

Before comparing this result with the velocity profile obtained from simulations, we emphasize two aspects. First, to obtain the result in Eq. (12), one assumes that the fluid is incompressible and the LJ system under consideration is not. However, the Navier–Stokes equation for a compressible fluid contains a term proportional to $\nabla \cdot \mathbf{u}$ that in our case is equal to zero because the flow is unidirectional along the x -direction and the magnitude of the flow velocity does not change along this axis. Second, the result in Eq. (12) was obtained by assuming that $\Delta p/\Delta x$ is constant. In our model, we need to verify that the constant pressure gradient induced in between the right and left reservoirs creates a constant pressure gradient across the AT region.

To compute the pressure, we discretize the simulation box in cubic cells of linear size 1σ and build the pressure profile by considering a sequence of cells aligned along the x -axis and located at a distance 5σ from the rigid surface. Hence, the structured layers of fluid close to the wall are not taken into account, which results in effectively counting the bulk contribution to the pressure. We compute the stress tensor per-atom S for particles instantaneously present in the cell. Finally, based on the Irvin–Kirkwood derivation,⁵⁴ we obtain the pressure tensor for every cell of volume V as $P = -(S_{xx} + S_{yy} + S_{zz})/3V$ ⁵⁵ and average contributions along the y and z directions to obtain the pressure as a function of x . We emphasize here that in case one requires a more precise calculation of the pressure tensor, especially close to inhomogeneous regions, it is essential to use the method of planes introduced in Ref. 31.

Plot of pressure profiles [Fig. 7(a)] for different induced densities, in the case of purely repulsive interaction with the walls, indicates that the pressure gradient is indeed constant. As a matter of fact, we find that there is a linear relation between the pressure difference measured across the AT region $p_R^{\text{AT}} - p_L^{\text{AT}}$ and the nominal pressure difference $p_R^{\text{IG}} - p_L^{\text{IG}}$ for different values of the induced density, as indicated in Fig. 7(b). The slope of the line is 0.47. This value coincides with the constant pressure gradient across the resolution, namely, $\frac{L_{\text{AT}}}{L_{\text{AT}} + 2L_{\text{HY}} + L_{\text{corr}}} = \frac{5}{10}$. The quantity $L_{\text{Corr}} = 20 \sigma$ measures the distance from the interface of the HY region to the left reservoir up to the point at which the pressure reaches the equilibrium pressure. The constant pressure gradient obtained in the AT region can be understood in terms of the virial expansion of the pressure in terms of the density for a LJ system, namely, relatively small gradients in density (of maximum $0.08 \sigma^{-4}$ here) induce ideal-gas-like response in the atomistic system.

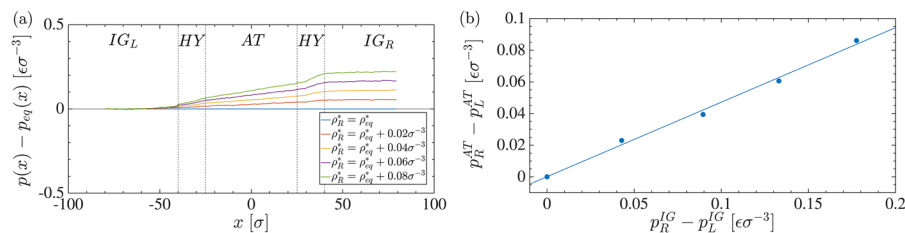


FIG. 7. (a) Difference of pressure profiles of the systems with respect to the equilibrium pressure profile $p(x) - p_{\text{eq}}(x)$. (b) Comparison between pressure difference of reservoirs $p_R^{\text{IG}} - p_L^{\text{IG}}$ and the pressure difference calculated at the boundary of atomistic region $p_R^{\text{AT}} - p_L^{\text{AT}}$.

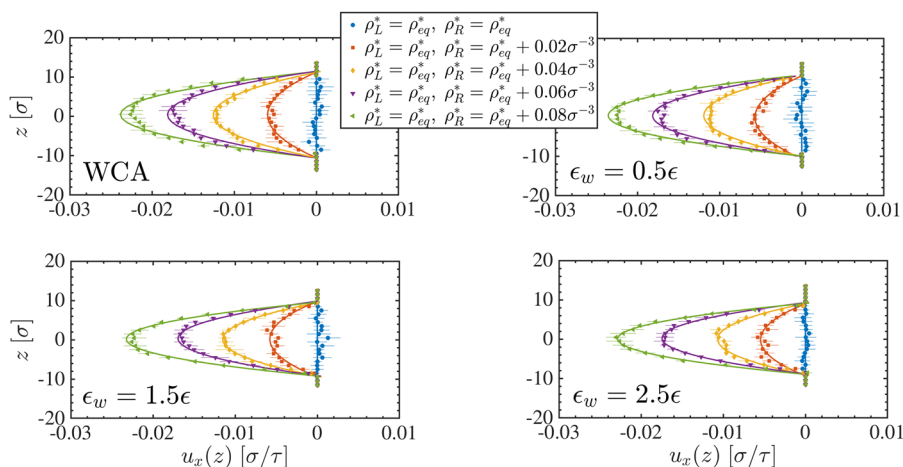


FIG. 8. Velocity profiles of the pressure driven flow are shown for different density gradients induced by controlling the density at the right reservoir (ρ_R^*). The density at the left reservoir is set to equilibrium density $\rho_L^* = \rho^{eq}$. The solid lines are the parabolic fitting to each set of data points.

To compare with the result expected from Eq. (12), we calculate the corresponding average of $u_x(z)$ in the atomistic region and obtain the velocity profiles plotted in Fig. 8 for all liquid–wall interactions. The solid lines represent the parabolic functions fitted to the data points. In all cases and apart from relatively small statistic fluctuations, the simulated velocities follow closely the expected parabolic profile.

The resulting velocity profile implies that the maximum velocity occurs at the center of the channel $-u_{max} = u_x(z = 0)$. This maximum velocity is linearly proportional to the nominal density difference, i.e., $u_{max} \propto (\rho_R^* - \rho_L^*)$, as presented in Fig. 9.

Finally, we can use u_{max} to compute the viscosity η as

$$\eta = \frac{\Delta P}{\Delta x} \frac{D_h^2}{4} u_{max}^{-1}.$$

For the WCA case, we use all the values of $\Delta P/\Delta x$ (Fig. 7) and u_{max} (Fig. 9), corresponding to the density imbalances considered in our study. We estimate $D_h = 19 \sigma$ from the density profiles in Fig. 3. Finally, we obtain $\eta = 6.3 \pm 0.6 \epsilon \sigma^{-3} \tau$. This result is comparable with the value obtained using Müller–Plathe’s method⁵⁶ ($\eta = 5.2$

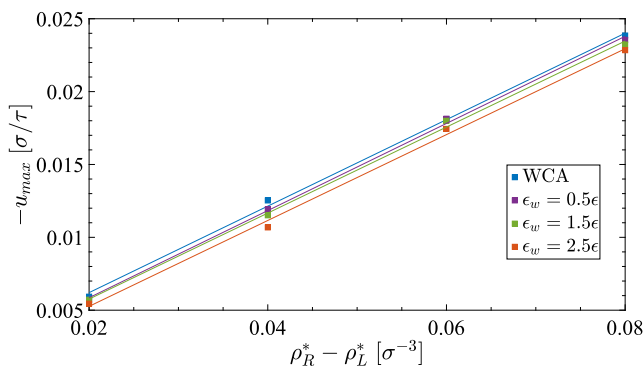


FIG. 9. Maximum velocity of the Poiseuille flow vs different relative densities between the reservoirs ($\rho_R^* - \rho_L^*$). The density at the left reservoir is set to equilibrium density $\rho_L^* = \rho^{eq}$. The solid lines are linear fits to the data points.

$\pm 0.3 \epsilon \sigma^{-3} \tau$). The discrepancy might be due to lack of statistics and the uncertainty related to the ambiguous definition of the volume accessible to the fluid, counted in the value of D_h .

IV. DISCUSSION AND CONCLUSIONS

In computer simulations, the investigation of a large closed system allows one to sample the grand canonical ensemble. A subdomain of volume V and an average number of particles $\langle N \rangle$ inside a system with a fixed number of particles N_0 and volume V_0 is considered to be in the grand canonical ensemble provided that the condition $V/V_0 \approx 0.01$ holds.⁴ For the Lennard-Jones systems investigated here, a subdomain of volume $V \sim (10 \sigma)^3$, with the estimate for the correlation length of the system as 10σ , would require $V_0 \sim 100 V$. With a density $\rho = 0.647 \sigma^{-3}$, the simulation would need $N_0 \sim 10^6$. This number is one order of magnitude larger than the number of particles considered here, which already highlights the advantage of using the proposed method. Additionally, we emphasize that a detailed assessment of the relative atomistic, hybrid, and ideal gas region sizes might suggest that we could further reduce the size of the system without affecting our main results.

Instead of the direct approach discussed above, it is perhaps more convenient to use one of the available grand canonical molecular dynamics methods.^{49–51,57–63} A common ingredient in most approaches consists of inserting particles with a given system-dependent probability. In general, when the system under consideration is simple in terms of the force field used for its description, or if the system is at low density/concentration conditions, this is the method of choice. Far away from such conditions, the particle insertion protocol becomes highly inefficient. In this respect, the adaptive resolution framework constitutes an alternative for existing methods. In particular, for the Hamiltonian adaptive resolution discussed in Ref. 24, the target system is in contact with a reservoir of ideal gas particles at constant temperature, volume, and by ensuring a uniform density across the simulation box, also at constant chemical potential. The combination with a particle insertion algorithm operating in the ideal gas region guarantees a reservoir of infinite size, thus completing the definition of grand canonical ensemble.

Therefore, the method proposed here is a robust strategy to perform open-boundary molecular dynamics simulations, mainly when the system under consideration is dense, or highly concentrated in the case of mixtures, and regardless of the complexity introduced by the force field description.

A straightforward change in the geometry and periodic boundary conditions in the simulation box allows one to decouple the ideal gas reservoir. Hence, it is possible to simultaneously impose different temperature, density, and concentration conditions on the system. In the particular case of induced density gradients,^{29,53,64–66} current non-equilibrium molecular dynamics methods include external forces that might introduce artifacts in the simulation resulting from non-conservation of linear momentum.⁶⁷ Instead, the method proposed here conserves, on average, momentum. Moreover, the simplicity of the reservoir gives the possibility to study different out-of-equilibrium conditions for complex molecular systems, which constitutes a significant improvement over state-of-the-art simulation methods.

In summary, in this work, we presented a method to perform open-boundary molecular dynamics simulations. We used the H-AdResS framework where the atomistic target system is in physical contact with a reservoir of non-interacting particles at constant temperature, volume, and chemical potential. In addition to the straightforward calculation of the chemical potential, the use of H-AdResS allows one to study liquid mixtures directly. In this context, we introduced a particle insertion/deletion algorithm that operates, at minimal computational expenses, on the ideal gas reservoir. Approaches exploiting similar ideas are available in the literature,^{58,68} however, they lack the flexibility provided by the coupling to the ideal gas system. The proposed method allows one to perform constant chemical potential simulations under various conditions. More importantly, by studying the pressure-driven flow through a channel, we showed that it is also possible to perform well-controlled non-equilibrium molecular dynamics simulations.

AUTHOR'S CONTRIBUTIONS

R.P. and R.C.-H. contributed equally to this work.

ACKNOWLEDGMENTS

The authors thank Pietro Ballone and Dominic Spiller for critical reading and insightful comments. M.H., K.K., R.P., and R.C.-H. gratefully acknowledge funding from SFB-TRR146 of the German Research Foundation (DFG). This work was supported by the European Research Council under the European Union's Seventh Framework Program (No. FP7/2007-2013)/ERC (Grant Agreement No. 340906-MOLPROCOMP). This project received funding from the European Research Council (ERC) under the European Union's Horizon 2020 research and innovation program (Grant No. 758588).

DATA AVAILABILITY

The data that support the findings of this study are available from the corresponding author upon reasonable request.

REFERENCES

- 1 J. Cervera, M. A. Gilabert, and J. A. Manzanares, "Liquid-vapor coexistence and the PVT surface of a lattice fluid," *Am. J. Phys.* **79**, 206 (2011).
- 2 F. Román, J. White, A. González, and S. Velasco, "Ensemble effects in small systems," in *Theory and Simulation of Hard-Sphere Fluids and Related Systems* (Springer Berlin Heidelberg, Berlin, Heidelberg, 2008), pp. 343–381.
- 3 M. Rovere, D. W. Heermann, and K. Binder, "The gas-liquid transition of the two-dimensional Lennard-Jones fluid," *J. Phys.: Condens. Matter* **2**, 7009 (1990).
- 4 M. Heidari, K. Kremer, R. Potestio, and R. Cortes-Huerto, "Finite-size integral equations in the theory of liquids and the thermodynamic limit in computer simulations," *Mol. Phys.* **116**, 3301 (2018).
- 5 M. Praprotnik, L. Delle Site, and K. Kremer, "Adaptive resolution molecular-dynamics simulation: Changing the degrees of freedom on the fly," *J. Chem. Phys.* **123**, 224106 (2005).
- 6 M. Praprotnik, L. Delle Site, and K. Kremer, "Adaptive resolution scheme for efficient hybrid atomistic-mesoscale molecular dynamics simulations of dense liquids," *Phys. Rev. E* **73**, 066701 (2006).
- 7 M. Praprotnik, L. Delle Site, and K. Kremer, "A macromolecule in a solvent: Adaptive resolution molecular dynamics simulation," *J. Chem. Phys.* **126**, 134902 (2007).
- 8 M. Praprotnik, L. Delle Site, and K. Kremer, "Multiscale simulation of soft matter: From scale bridging to adaptive resolution," *Annu. Rev. Phys. Chem.* **59**, 545 (2008).
- 9 S. Fritsch, C. Junghans, and K. Kremer, "Structure formation of toluene around C60: Implementation of the adaptive resolution scheme (AdResS) into GRO-MACS," *J. Chem. Theory Comput.* **8**, 398 (2012).
- 10 R. Delgado-Buscalioni, K. Kremer, and M. Praprotnik, "Concurrent triple-scale simulation of molecular liquids," *J. Chem. Phys.* **128**, 114110 (2008).
- 11 S. Fritsch, S. Poblete, C. Junghans, G. Ciccotti, L. Delle Site, and K. Kremer, "Adaptive resolution molecular dynamics simulation through coupling to an internal particle reservoir," *Phys. Rev. Lett.* **108**, 170602 (2012).
- 12 D. Mukherji and K. Kremer, "Coil-globule-coil transition of PNIPAm in aqueous methanol: Coupling all-atom simulations to semi-grand canonical coarse-grained reservoir," *Macromolecules* **46**, 9158 (2013).
- 13 H. Wang, C. Hartmann, C. Schütte, and L. Delle Site, "Grand-canonical-like molecular-dynamics simulations by using an adaptive-resolution technique," *Phys. Rev. X* **3**, 011018 (2013).
- 14 A. Agarwal, J. Zhu, C. Hartmann, H. Wang, and L. D. Site, "Molecular dynamics in a grand ensemble: Bergmann-Lebowitz model and adaptive resolution simulation," *New J. Phys.* **17**, 083042 (2015).
- 15 L. Delle Site, C. Krekeler, J. Whittaker, A. Agarwal, R. Klein, and F. Höfling, "Molecular dynamics of open systems: Construction of a mean-field particle reservoir," *Adv. Theory Simul.* **2**, 1900014 (2019).
- 16 A. Agarwal, H. Wang, C. Schütte, and L. D. Site, "Chemical potential of liquids and mixtures via adaptive resolution simulation," *J. Chem. Phys.* **141**, 034102 (2014).
- 17 R. Delgado-Buscalioni, K. Kremer, and M. Praprotnik, "Coupling atomistic and continuum hydrodynamics through a mesoscopic model: Application to liquid water," *J. Chem. Phys.* **131**, 244107 (2009).
- 18 U. Alekseeva, R. G. Winkler, and G. Sutmoller, "Hydrodynamics in adaptive resolution particle simulations: Multiparticle collision dynamics," *J. Comput. Phys.* **314**, 14 (2016).
- 19 R. Delgado-Buscalioni, J. Sablić, and M. Praprotnik, "Open boundary molecular dynamics," *Eur. Phys. J.: Spec. Top.* **224**, 2331 (2015).
- 20 L. D. Site and M. Praprotnik, "Molecular systems with open boundaries: Theory and simulation," *Phys. Rep.* **693**, 1 (2017).
- 21 J. Zavadlav, J. Sablić, R. Podgornik, and M. Praprotnik, "Open-boundary molecular dynamics of a DNA molecule in a hybrid explicit/implicit salt solution," *Biophys. J.* **114**, 2352 (2018).
- 22 R. Potestio, S. Fritsch, P. Español, R. Delgado-Buscalioni, K. Kremer, R. Everaers, and D. Donadio, "Hamiltonian adaptive resolution simulation for molecular liquids," *Phys. Rev. Lett.* **110**, 108301 (2013).
- 23 R. Potestio, P. Español, R. Delgado-Buscalioni, R. Everaers, K. Kremer, and D. Donadio, "Monte Carlo adaptive resolution simulation of multicomponent molecular liquids," *Phys. Rev. Lett.* **111**, 060601 (2013).

- ²⁴M. Heidari, K. Kremer, R. Cortes-Huerto, and R. Potestio, "Spatially resolved thermodynamic integration: An efficient method to compute chemical potentials of dense fluids," *J. Chem. Theory Comput.* **14**, 3409 (2018).
- ²⁵C. Perego, F. Giberti, and M. Parrinello, "Chemical potential calculations in dense liquids using metadynamics," *Eur. Phys. J.: Spec. Top.* **225**, 1621 (2016).
- ²⁶M. Radu and K. Kremer, "Enhanced crystal growth in binary Lennard-Jones mixtures," *Phys. Rev. Lett.* **118**, 055702 (2017).
- ²⁷T. Karmakar, P. M. Piaggi, C. Perego, and M. Parrinello, "A cannibalistic approach to grand canonical crystal growth," *J. Chem. Theory Comput.* **14**, 2678 (2018).
- ²⁸D. J. Evans and G. P. Morriss, "Shear thickening and turbulence in simple fluids," *Phys. Rev. Lett.* **56**, 2172 (1986).
- ²⁹U. Heinbuch and J. Fischer, "Liquid flow in pores: Slip, no-slip, or multilayer sticking," *Phys. Rev. A* **40**, 1144 (1989).
- ³⁰P. A. Thompson and M. O. Robbins, "Shear flow near solids: Epitaxial order and flow boundary conditions," *Phys. Rev. A* **41**, 6830 (1990).
- ³¹B. D. Todd, D. J. Evans, and P. J. Daivis, "Pressure tensor for inhomogeneous fluids," *Phys. Rev. E* **52**, 1627 (1995).
- ³²J.-L. Barrat and L. Bocquet, "Large slip effect at a nonwetting fluid-solid interface," *Phys. Rev. Lett.* **82**, 4671 (1999).
- ³³J.-L. Barrat and L. Bocquet, "Influence of wetting properties on hydrodynamic boundary conditions at a fluid/solid interface," *Faraday Discuss.* **112**, 119 (1999).
- ³⁴C. Denniston and M. O. Robbins, "Molecular and continuum boundary conditions for a miscible binary fluid," *Phys. Rev. Lett.* **87**, 178302 (2001).
- ³⁵C. Denniston and M. O. Robbins, "General continuum boundary conditions for miscible binary fluids from molecular dynamics simulations," *J. Chem. Phys.* **125**, 214102 (2006).
- ³⁶L. Guo, S. Chen, and M. O. Robbins, "Effective slip boundary conditions for sinusoidally corrugated surfaces," *Phys. Rev. Fluids* **1**, 074102 (2016).
- ³⁷Y. Liu, R. Ganti, H. G. A. Burton, X. Zhang, W. Wang, and D. Frenkel, "Microscopic Marangoni flows cannot be predicted on the basis of pressure gradients," *Phys. Rev. Lett.* **119**, 224502 (2017).
- ³⁸L. Fu, S. Merabia, and L. Joly, "What controls thermo-osmosis? Molecular simulations show the critical role of interfacial hydrodynamics," *Phys. Rev. Lett.* **119**, 214501 (2017).
- ³⁹H. Yoshida, S. Marbach, and L. Bocquet, "Osmotic and diffusio-osmotic flow generation at high solute concentration II. Molecular dynamics simulations," *J. Chem. Phys.* **146**, 194702 (2017).
- ⁴⁰R. Ganti, Y. Liu, and D. Frenkel, "Molecular simulation of thermo-osmotic slip," *Phys. Rev. Lett.* **119**, 038002 (2017).
- ⁴¹R. Ganti, Y. Liu, and D. Frenkel, "Hamiltonian transformation to compute thermo-osmotic forces," *Phys. Rev. Lett.* **121**, 068002 (2018).
- ⁴²Y. Liu, R. Ganti, and D. Frenkel, "Pressure gradients fail to predict diffusio-osmosis," *J. Phys.: Condens. Matter* **30**, 205002 (2018).
- ⁴³K. Kreis, A. C. Fogarty, K. Kremer, and R. Potestio, "Advantages and challenges in coupling an ideal gas to atomistic models in adaptive resolution simulations," *Eur. Phys. J.: Spec. Top.* **224**, 2289 (2015).
- ⁴⁴S. Plimpton, "Fast parallel algorithms for short-range molecular dynamics," *J. Comput. Phys.* **117**, 1 (1995).
- ⁴⁵M. Heidari, R. Cortes-Huerto, D. Donadio, and R. Potestio, "Accurate and general treatment of electrostatic interaction in Hamiltonian adaptive resolution simulations," *Eur. Phys. J.: Spec. Top.* **225**, 1505 (2016).
- ⁴⁶P. Español, R. Delgado-Buscalioni, R. Everaers, R. Potestio, D. Donadio, and K. Kremer, "Statistical mechanics of Hamiltonian adaptive resolution simulations," *J. Chem. Phys.* **142**, 064115 (2015).
- ⁴⁷B. Widom, "Structure of interfaces from uniformity of the chemical potential," *J. Stat. Phys.* **19**, 563 (1978).
- ⁴⁸L. D. Landau and E. M. Lifshitz, *Statistical Physics*, 3rd ed. (Pergamon, Oxford, 1980).
- ⁴⁹D. Frenkel and B. Smit, *Understanding Molecular Simulation: From Algorithms to Applications*, 2nd ed. (Academic Press, 2002).
- ⁵⁰S. Boinepalli and P. Attard, "Grand canonical molecular dynamics," *J. Chem. Phys.* **119**, 12769 (2003).
- ⁵¹H. Eslami and F. Müller-Plathe, "Molecular dynamics simulation in the grand canonical ensemble," *J. Comput. Chem.* **28**, 1763 (2007).
- ⁵²S. Stalter, L. Yelash, N. Emamy, A. Statt, M. Hanke, M. Lukáčová-Medvid'ová, and P. Virnau, "Molecular dynamics simulations in hybrid particle-continuum schemes: Pitfalls and caveats," *Comput. Phys. Commun.* **224**, 198 (2018).
- ⁵³Q. D. To, T. T. Pham, G. Lauriat, and C. Léonard, "Molecular dynamics simulations of pressure-driven flows and comparison with acceleration-driven flows," *Adv. Mech. Eng.* **4**, 580763 (2012).
- ⁵⁴J. H. Irving and J. G. Kirkwood, "The statistical mechanical theory of transport processes. IV. The equations of hydrodynamics," *J. Chem. Phys.* **18**, 817 (1950).
- ⁵⁵A. P. Thompson, S. J. Plimpton, and W. Mattson, "General formulation of pressure and stress tensor for arbitrary many-body interaction potentials under periodic boundary conditions," *J. Chem. Phys.* **131**, 154107 (2009).
- ⁵⁶F. Müller-Plathe, "Reversing the perturbation in nonequilibrium molecular dynamics: An easy way to calculate the shear viscosity of fluids," *Phys. Rev. E* **59**, 4894 (1999).
- ⁵⁷D. J. Adams, "Grand canonical ensemble Monte Carlo for a Lennard-Jones fluid," *Mol. Phys.* **29**, 307 (1975).
- ⁵⁸T. Çagin and B. M. Pettitt, "Grand molecular dynamics: A method for open systems," *Mol. Simul.* **6**, 5 (1991).
- ⁵⁹A. Papadopoulou, E. D. Becker, M. Lupkowski, and F. van Swol, "Molecular dynamics and Monte Carlo simulations in the grand canonical ensemble: Local vs global control," *J. Chem. Phys.* **98**, 4897 (1993).
- ⁶⁰G. C. Lynch and B. M. Pettitt, "Grand canonical ensemble molecular dynamics simulations: Reformulation of extended system dynamics approaches," *J. Chem. Phys.* **107**, 8594 (1997).
- ⁶¹A. P. Thompson, D. M. Ford, and G. S. Heffelfinger, "Direct molecular simulation of gradient-driven diffusion," *J. Chem. Phys.* **109**, 6406 (1998).
- ⁶²R. M. Shroll and D. E. Smith, "Molecular dynamics simulations in the grand canonical ensemble: Formulation of a bias potential for umbrella sampling," *J. Chem. Phys.* **110**, 8295 (1999).
- ⁶³A. Malasics, D. Gillespie, and D. Boda, "Simulating prescribed particle densities in the grand canonical ensemble using iterative algorithms," *J. Chem. Phys.* **128**, 124102 (2008).
- ⁶⁴B. D. Todd and P. J. Daivis, *Nonequilibrium Molecular Dynamics* (Cambridge University Press, 2017).
- ⁶⁵L. Hannon, G. C. Lie, and E. Clementi, "Molecular dynamics simulation of channel flow," *Phys. Lett. A* **119**, 174 (1986).
- ⁶⁶J. Koplik, J. R. Banavar, and J. F. Willemsen, "Molecular dynamics of fluid flow at solid surfaces," *Phys. Fluids A* **1**, 781 (1989).
- ⁶⁷B. Dünweg, "Molecular dynamics algorithms and hydrodynamic screening," *J. Chem. Phys.* **99**, 6977 (1993).
- ⁶⁸R. F. Cracknell, D. Nicholson, and N. Quirke, "Direct molecular dynamics simulation of flow down a chemical potential gradient in a slit-shaped micropore," *Phys. Rev. Lett.* **74**, 2463 (1995).